Creation of high-dimensional entanglement of polar molecules via optimal control fields

Zuo-Yuan Zhang[1,*] and Jin-Ming Liu [2,†]

[1]*College of Physical Science and Technology, Yangzhou University, Yangzhou, 225009, China*
[2]*State Key Laboratory of Precision Spectroscopy, School of Physics and Electronic Science,*
East China Normal University, Shanghai 200241, China

Quantum entanglement in high-dimensional Hilbert space offers broad prospects for quantum information science. Polar molecules have a rich internal structure and long coherence time, serving as an attractive candidate for quantum information processing. In this paper, we propose a theoretical scheme for creating high-dimensional entangled states based on ultracold SrO molecules. Qudits are encoded in the pendular states induced by an external electric field and coupled by the dipole-dipole interaction. With the assistance of optimal control theory, a series of optimal microwave fields is designed for the generation of an entangled qutrit-qubit state, qutrit-qutrit state, and ququart-ququart state through numerical iterations. We detail the relation of the fidelity and entanglement of the systemic final states with the number of iteration steps after the control fields are applied and analyze the population dynamics of the field-driven wave functions during time evolution. Moreover, three coupled SrO molecules arranged in an equilateral triangle configuration are employed as pendular qubits, and the trimolecular *W* and Greenberger-Horne-Zeilinger states are realized with high fidelities by optimal control. The specific molecule and experimental parameters used in our theoretical studies are chosen for computational convenience, but we include a discussion of how our results can be applied to realistic situations as well. In principle, our results could be extended to a situation with more pendular qudits, providing a significant step toward the achievement of high-dimensional quantum information processing with arrays of polar molecules.

I. INTRODUCTION

Quantum information science has arisen over the past several decades and has shown potential applications in wide fields. Recently, there has been growing interest in quantum communication and computation in large Hilbert spaces [1–3]. This is due to the fact that higher-dimensional systems can offer a larger code space, which contributes to enhancing the capacity of the communication channel [4], the security of quantum cryptography [5], resistance to noise [6,7], etc. Generally speaking, one way of enlarging Hilbert spaces is to increase the number of qubits; another way is to employ *d*-level systems as qudits. Note that polar molecules have a rich inner energy structure, which can be used to encode a large amount of quantum information [8–14]. For example, Sawant *et al.* [14] examined the rotational and hyperfine structure of ultracold molecules in electronic states of $^2\Sigma$ and $^1\Sigma$ symmetry and identified possible implementations of four-level qudits in both CaF and RbCs. On the other hand, polar molecules can be coupled by the long-range dipole-dipole interaction, offering a feasible path to the implementation of scalable quantum computation [15,16]. In our previous studies, three-qubit quantum logic gates were successfully simulated by using three dipole-coupled molecules [17], and they can be further generalized to the situation of *N* qubits.

Moreover, methods and techniques for cooling, trapping, and controlling molecules such as SrF, CaF, and YO have made enormous progress in recent years [18–22]. As a result, arrays of ultracold trapped polar molecules have become one of the most promising carriers in quantum information processing. As early as 2002, DeMille [8] offered a seminal proposal for realizing quantum computation by encoding the qubits in the electric dipole moments of diatomic molecules, which are trapped in the optical lattice and oriented by the external electric field. Moreover, Yelin *et al.* [23] showed how to switch on and off strong dipole-dipole interactions and investigated the implementation of two-qubit gates in diatomic polar molecules. Recently, Yu *et al.* [24] proposed a scalable platform for quantum computing based on symmetric-top molecules, in which the fidelities can approach the threshold for fault-tolerant quantum computing under realistic experimental conditions.

It is well accepted that quantum entanglement is a significant physical resource in the field of quantum information. Up to now, many efforts have been devoted to exploring the entanglement and coherence of molecular systems [25–32]. For instance, Wei *et al.* [25] analyzed the relations between the entanglement of the pendular qubit states for two linear molecules and the electric field, dipole-dipole interaction, and ambient temperature. Chae [31] proposed a theoretical scheme for the entanglement of MgF molecules in an optical tweezer array via rotational blockade. However, studies seldom involve high-dimensional entanglement of molecular systems. As we know, high-dimensional entanglement has

---
*Corresponding author: zy.zhang@yzu.edu.cn
†Corresponding author: jmliu@phy.ecnu.edu.cn

more advantages for long-distance communication [33,34], quantum distillation [35], the Bell-test experiment [36], and quantum computation [37], and entangled states in high-dimensional spaces have been created in atomic ensembles [38–40], integrated platforms [41], rare-earth-doped crystals [42,43], etc. In this paper, we study how to create entangled qubit, qutrit, and ququart (four-level qudit) states with pendular states in SrO molecules coupled by dipole-dipole interaction. To achieve the addressability of the pendular qudit states, the SrO molecules are assumed to be located in the external electric field with an appreciable gradient. Meanwhile, we also achieve the trimolecular entangled W state and Greenberger-Horne-Zeilinger (GHZ) state with high fidelities. The method we adopt here is the optimal control theory (OCT) [44]. OCT is an effective approach to find the optimal solution for a physical problem under constraint conditions, which can be used to design control fields for the generation of intermolecular entanglement [30,32,45]. Recently, Hughes *et al.* [32] designed an entangling gate for polar molecules by employing the tunable dipole-dipole interaction together with a microwave (MW) field. The MW field is shaped by the gradient ascent pulse engineering algorithm, and the fidelity of the entangling gate can reach very high values for wide regions of the parameter space. Furthermore, they considered the thermal motional excitations. The optimized MW field can drive the system that is initially in a product state of internal and excited motional states into the high-fidelity target state in the presence of incoherent motional excitation. Here, we adopt the OCT to design a series of MW pulses for pendular states of SrO molecules, which can drive the transitions of molecular systems from the separable ground states into the high-dimensional entangled states. Our results could shed some light on the generation of entanglement resource in high dimensions and the construction of the high-capacity quantum network based on polar molecules.

The outline of this paper is organized as follows. In Sec. II we give a brief review of the model of dipole-dipole-coupled polar molecules in pendular states and introduce the method of optimal control. The results of the simulations are given in Sec. III, including the creation of qudit-qudit entanglement and three-qubit entanglement. We close in Sec. IV with a summary of the results.

II. THEORY

A. Model

For N identical trapped polar linear molecules coupled via the dipole-dipole interaction, the Hamiltonian is [15]

$$H = \sum_{i=1}^{N} H_i + \sum_{i=1}^{N-1} \sum_{j=i+1}^{N} V_{d-d}^{i,j}, \tag{1}$$

with

$$H_i = \frac{p_i^2}{2m} + V_{\text{trap}}(\mathbf{r}_i) + B\mathbf{J}_i^2 - \boldsymbol{\mu} \cdot \boldsymbol{\varepsilon} \tag{2}$$

and

$$V_{d-d}^{i,j} = \frac{\boldsymbol{\mu}_i \cdot \boldsymbol{\mu}_j - 3(\boldsymbol{\mu}_i \cdot \mathbf{n})(\boldsymbol{\mu}_j \cdot \mathbf{n})}{|\mathbf{r}_i - \mathbf{r}_j|^3}. \tag{3}$$
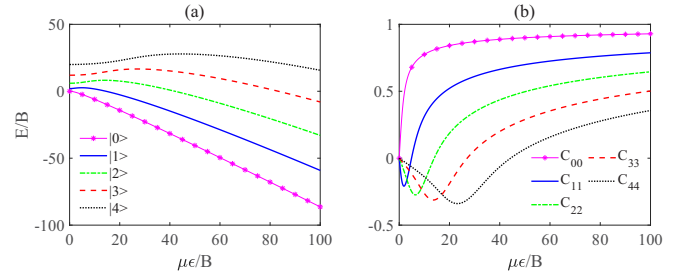

FIG. 1. (a) Pendular energy levels (in terms of the rotational constant B) of an ultracold polar molecule in the electric field for $M = 0$ as a function of $\mu\varepsilon/B$, which are encoded as the qudit $|q\rangle$ with $q = 0, 1, 2, 3, 4$. (b) Molecular orientation C_{qq} as a function of $\mu\varepsilon/B$.

Here, H_i is the Hamiltonian of the ith polar molecule oriented by a static electric field $\boldsymbol{\varepsilon}$ and trapped in a well with potential energy V_{trap}. The parameters m, B, and μ denote the molecular mass, the rotational constant, and the permanent dipole moment, respectively. The term $p_i^2/2m$ characterizes the translational kinetic energy of the molecule, whereas $B\mathbf{J}_i^2$ characterizes the rotational energy with the molecular angular momentum $\mathbf{J}_i$. Moreover, $V_{d-d}^{i,j}$ denotes the dipole-dipole interaction between the ith and the jth molecules, with $\mathbf{n}$ being a unit vector along $\mathbf{r}_{ij}$, where $|\mathbf{r}_{ij}| = |\mathbf{r}_i - \mathbf{r}_j|$ denotes the intermolecular distance. For the ultracold polar molecules trapped in the potential well, the translational motion is quite modest and very nearly harmonic [25]. For simplicity, in this paper we do not consider the translational kinetic energy $p_i^2/2m$ and the potential energy V_{trap}. As a result, the Hamiltonian for a single molecule is reduced to the following form:

$$H_i = B\mathbf{J}_i^2 - \mu\varepsilon \cos\theta, \tag{4}$$

where θ is the angle between the dipole moment $\boldsymbol{\mu}$ and the electric field $\boldsymbol{\varepsilon}$. Under strong external electric field, the polar molecules are induced to undergo pendular oscillation along the field axis over a limited angular range, leading to the creation of pendular states [46]. In Fig. 1(a), several energy levels of a linear molecule in pendular states for $M = 0$ are plotted as a function of $\mu\varepsilon/B$, where M is the projection of $\mathbf{J}_i$ in the direction of the electric field. For a d-level molecular system, the pendular states versus the energy levels in ascending order are encoded to be the qudit $|q\rangle$, with $q = 0, 1, 2, \ldots, d$. Indeed, the pendular qudit state $|q\rangle$ can be regarded as the superposition of field-free rotational states, i.e., $|q\rangle = \sum_{l=0}^{\infty} c_l |J_i = l, M = 0\rangle$, where c_l are the coefficients of sums of rotational states. It should be mentioned that the scheme we adopted here is actually an extension of DeMille's proposal [8] from a two-level pendular qubit to a d-level qudit. Furthermore, for $M = 0$ the dipole-dipole interaction shown in Eq. (3) can be simplified by averaging the azimuthal angles to [25,30]

$$V_{d-d}^{i,j} = \Omega(1 - 3\cos^2\alpha)\cos\theta_i\cos\theta_j. \tag{5}$$

Here, $\Omega = \mu^2/r_{ij}^3$, θ_m ($m = i, j$) is the angle between the field direction and the mth molecular axis, and α is the angle

between the field direction and the vector $\mathbf{r}_{ij}$. In the following we assume that the electric field is perpendicular to the vector $\mathbf{r}_{ij}$, i.e., $\alpha = \pi/2$.

In the Hilbert space consisting of pendular qudits $|q_1, q_2, \ldots, q_N\rangle$ of N polar molecules, the Hamiltonian H_i for the ith molecule can be expanded as

$$H_i = I_1 \otimes I_2 \otimes \cdots \otimes I_{i-1} \otimes \begin{pmatrix} E_0^i & 0 & \ldots & 0 \\ 0 & E_1^i & \ldots & 0 \\ \vdots & \vdots & \ddots & \vdots \\ 0 & 0 & \ldots & E_d^i \end{pmatrix} \otimes I_{i+1} \otimes \cdots \otimes I_N, \tag{6}$$

where I_k $(k = 1, 2, \ldots, N)$ represents the identity matrix and $E_0^i, E_1^i, \ldots, E_d^i$ represent the eigenenergies versus the pendular qudit states $|0\rangle, |1\rangle, \ldots, |d\rangle$, respectively. Similarly, the dipole-dipole interaction $V_{d-d}^{i,j}$ can be expanded as

$$V_{d-d}^{i,j} = \Omega \times I_1 \otimes \cdots \otimes I_{i-1} \otimes \begin{pmatrix} C_{00}^i & C_{01}^i & \ldots & C_{0d}^i \\ C_{10}^i & C_{11}^i & \ldots & C_{1d}^i \\ \vdots & \vdots & \ddots & \vdots \\ C_{d0}^i & C_{d1}^i & \ldots & C_{dd}^i \end{pmatrix} \otimes I_{i+1} \otimes \cdots \otimes I_{j-1} \otimes \begin{pmatrix} C_{00}^j & C_{01}^j & \ldots & C_{0d}^j \\ C_{10}^j & C_{11}^j & \ldots & C_{1d}^j \\ \vdots & \vdots & \ddots & \vdots \\ C_{d0}^j & C_{d1}^j & \ldots & C_{dd}^j \end{pmatrix} \otimes I_{j+1} \otimes \cdots \otimes I_N. \tag{7}$$

Here, the matrix elements are defined by $C_{qq}^{i(j)} = \langle q | \cos\theta_{i(j)} | q \rangle$ and $C_{pq}^{i(j)} = \langle p | \cos\theta_{i(j)} | q \rangle$, with $q \neq p$. Note that the diagonal elements of the matrices actually characterize the orientations of the polar molecules in the electric field, which are displayed as a function of $\mu\varepsilon/B$ in Fig. 1(b).

B. Method

In this study, we use OCT to design optimal MW fields that interact with the polar molecules for the creation of high-dimensional entangled states. As we know, OCT is a common method in the fields of molecular quantum computation [17,47–50], molecular orientation and alignment [45,51,52], and discrimination of isotopologues in a mixture [53]. In general, it has an objective function [44,48]:

$$\mathbf{J}_{fi}[\psi_i(t), \psi_f(t), \mathbf{E}(t)]$$

$$= |\langle \psi_i(T) | \phi_f(T) \rangle|^2 - 2\text{Re}\Bigg\{ \langle \psi_i(T) | \phi_f(T) \rangle$$

$$\times \int_0^T \langle \psi_f(t) | \frac{\partial}{\partial t} + \frac{i}{\hbar} [H - \boldsymbol{\mu} \cdot \mathbf{E}(t)] | \psi_i(t) \rangle dt \Bigg\}$$

$$- \alpha_0 \times \int_0^T \frac{[\mathbf{E}(t)]^2}{S(t)} dt. \tag{8}$$

Here, $\psi_i(t)$ and $\psi_f(t)$ are the wave functions propagated forward and backward in time, respectively, both of which are driven by the control field $\mathbf{E}(t)$ with duration T. $\phi_f(T)$ is the desired target state, as well as the initial wave function of $\psi_f(t)$ at $t = T$. Moreover, the envelope function $S(t) = \sin^2(\pi t/T)$ guarantees the experimentally appropriate slow turn-on and turn-off pulse envelope. In addition, the parameter α_0 denotes the penalty factor, which is set as 1×10^5 to restrict the intensity of the control field in this paper. To maximize the objective function, $\delta\mathbf{J}_{fi} = 0$ is required. Then, a set of time-dependent coupled Schrödinger equations is

given by [44]

$$i\hbar \frac{\partial}{\partial t} \psi_i(t) = [H - \boldsymbol{\mu} \cdot \mathbf{E}(t)] \psi_i(t),$$

$$\psi_i(0) = \varphi_i(0),$$

$$i\hbar \frac{\partial}{\partial t} \psi_f(t) = [H - \boldsymbol{\mu} \cdot \mathbf{E}(t)] \psi_f(t),$$

$$\psi_f(T) = \phi_f(T). \tag{9}$$

Here, $\varphi_i(0)$ is the initial wave function of $\psi_i(t)$ at $t = 0$, and the control field $E(t)$ takes the following form:

$$E(t) = -\frac{\mu S(t)}{\hbar \alpha_0} \text{Im}\{\langle \psi_i(t) | \psi_f(t) \rangle \langle \psi_f(t) | \Lambda | \psi_i(t) \rangle\}, \tag{10}$$

with $\Lambda = \sum_{i=1}^N \cos\theta_i$. In what follows, Eq. (9) is numerically calculated by using the fourth-order Runge-Kutta algorithm. Furthermore, the rapidly converging iteration method is employed to optimize the control field, which can approach the converging limit within a few steps.

III. RESULTS

In this section, we focus on the optimization of the control fields interacting with the single-molecule system, bimolecule system, and trimolecule system to achieve the desired high-dimensional quantum states. In general, polar molecules with larger dipole moments can be oriented more easily in the external electric field. Moreover, under the same molecule spacing, the larger the dipole moments are, the stronger the dipole-dipole interaction between the molecules is. Thus, in this study we choose the SrO molecule as a suitable carrier, for which the body-fixed dipole moment μ is 8.9 debye and the rotational constant B is 0.33 cm^{-1}.
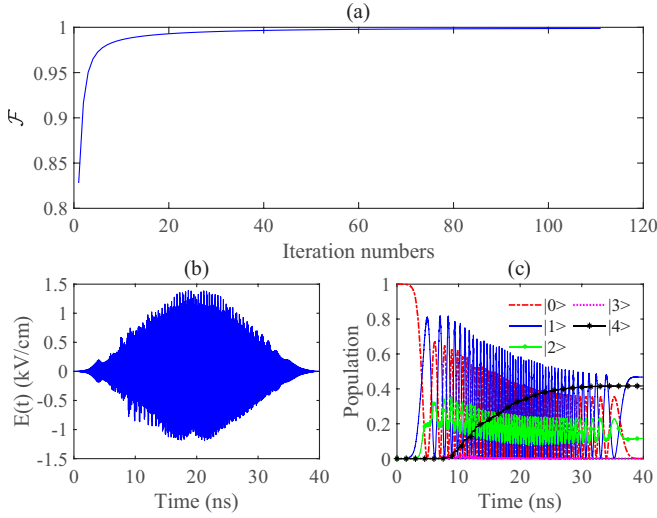
FIG. 2. (a) Fidelity of the systemic final state after applying the optimized control field for the transition of $\psi_i(t=0) = |0\rangle \rightarrow \phi_f(T) = \frac{2}{3}|1\rangle + \frac{1}{3}|2\rangle + \frac{2}{3}|4\rangle$ as a function of the iteration number. (b) Converged laser pulse corresponding to the last iteration, for which the maximum amplitude is about 1.39 kV/cm. (c) Time-dependent populations of the wave function driven by the converged laser pulse for creating the target state $\phi_f(T) = \frac{2}{3}|1\rangle + \frac{1}{3}|2\rangle + \frac{2}{3}|4\rangle$.

A. Single-qudit system

To show the feasibility of creating any desired target states in high-dimensional Hilbert space using OCT, we first take a single SrO molecule with five pendular energy levels [see Fig. 1(a)] as a special example. The SrO molecule is assumed to be located in the electric field $\boldsymbol{\varepsilon}$ with a strength of 2.2 kV/cm, corresponding to $\mu\varepsilon/B = 1$. Moreover, the initial state is set to the lowest pendular state, namely, $\psi_i(t=0) = |0\rangle$, and the target state is set to an arbitrary superposition state, namely, $\phi_f(T) = \sum_{q=0}^{4} c_q |q\rangle$. Without loss of generality, the coefficients c_q are supposed to be $c_0 = c_3 = 0$, $c_1 = c_4 = \frac{2}{3}$, and $c_2 = \frac{1}{3}$. Accordingly, the initial control field (in kV/cm) is guessed to be $E(t) = \sin^2(\pi t/T)\cos(\omega_{01}t)$ with duration $T = 40$ ns, where $\omega_{01} \approx 2\pi \times 2.22 \times 10^{10}$ rad/s is the transition frequency between the pendular states $|0\rangle$ and $|1\rangle$. Figure 2(a) shows the fidelity of the final state $\psi_i(t=T)$ corresponding to the transition of $|0\rangle \rightarrow \frac{2}{3}|1\rangle + \frac{1}{3}|2\rangle + \frac{2}{3}|4\rangle$ as a function of iteration number. Here, the fidelity is defined as $\mathcal{F} = |\langle\psi_i(T)|\phi_f(T)\rangle|^2$, which is the overlap between the systemic final state after the control field is applied and the target state we want. It can be seen from Fig. 2(a) that the fidelity is enhanced with the increase of the iteration number. If the convergence criterion is set to $\delta\mathcal{F} = 10^{-5}$, the iteration will terminate after 111 iteration steps, and the value of the fidelity can reach 0.999, where $\delta\mathcal{F}$ is the difference in the fidelities with respect to the adjacent iteration numbers. Figure 2(b) plots the converged control field, which is obtained by optimizing the initial field repeatedly. As shown in Fig. 2(c), under the converged control field the population of the initial state $|0\rangle$ evolves to 2.51×10^{-4} from 1, whereas those of $|1\rangle$, $|2\rangle$, $|3\rangle$, and $|4\rangle$ evolve to approximate values of 0.467, 0.116, 7.78×10^{-14}, and 0.416 from the initial value of zero, respectively, nearly meeting the ideal values versus the target

state $\phi_f(T)$. The superposition state for a single molecule is not entangled; however, from the perspective of coherence resource theory [54], the systemic coherence is still enhanced with the help of the optimal control field.

B. Qudit-qudit system

Now, we attempt to study the generation of the high-dimensional entanglement between two dipole-dipole-coupled SrO molecules. The intermolecular distance is set to 75 nm, and the strengths of the electric field acting on the two molecules are set to 4.4 and 6.6 kV/cm. Here, the appreciable gradient of the electric field enables the pendular qubits' addressability. In view of the fact that the hybrid qutrit-qubit state is the first nontrivial extension beyond the qubit-qubit case, the control field for the bipartite qutrit-qubit system needs to be optimized first. We assume that the pendular qutrits $|0\rangle$, $|1\rangle$, and $|2\rangle$ are encoded in the first SrO molecule, and the pendular qubits $|0\rangle$ and $|1\rangle$ are encoded in the second SrO molecule. To quantify the entanglement of the qutrit-qubit state, we introduce the concept of *negativity*. It is a measure of entanglement for arbitrary bipartite system, which is defined as [55]

$$\mathcal{N}(\rho) = \sum_i |\lambda_i(\rho^{T_A})| - 1, \qquad (11)$$

where ρ is the density matrix of a bipartite state and $\lambda_i(\rho^{T_A})$ is the ith eigenvalue of the partial transpose matrix corresponding to subsystem A. In the limit of ultracold temperature, the polar molecules are populated in the ground state with high probability. Thus, the ground state can be supposed to be the initial state. However, based on the above parameter, the value of negativity for the ground state is on the order of 10^{-4}, implying that the entanglement is very weak and can almost be negligible. As a result, we simplify reasonably the initial state to the separable state $|00\rangle$. To enhance the entanglement of the qutrit-qubit system, an entangled state $\frac{1}{\sqrt{2}}(|01\rangle + |20\rangle)$ is set to the target state, for which the negativity $\mathcal{N} = 1$.

From Fig. 3(a), we can find that the fidelity and the negativity synchronously increase with the growth of iteration steps and converge to 0.989 and 0.984 after 237 iterations, respectively. The optimal control field versus the last iteration is shown in Fig. 3(b), which is optimized from the initial field $E(t) = \sin^2(\pi t/T)\cos(\omega t)$, with $\omega = 2\pi \times 3.532 \times 10^{10}$ rad/s and $T = 250$ ns. Compared with the situation of the single molecule, it can be seen that more iteration steps in the numerical calculation and a longer duration time of the control field are necessary in the situation of qutrit-qubit coupling. To visualize the transition among the pendular states of the SrO molecules under the optimal field, we display the dynamics of the population for the field-driven wave function in Fig. 3(c). It is clear that the population of initial state $|00\rangle$ transfers almost averagely to the states of $|01\rangle$ and $|20\rangle$, demonstrating the creation of entangled qutrit-qubit state $\frac{1}{\sqrt{2}}(|01\rangle + |20\rangle)$. Before the high-fidelity entangled state can be successfully created, multiple transitions among the pendular energy levels are necessary. Thus, in Fig. 3(c) we can observe that the populations continue oscillating during the time evolution. Moreover, other entangled
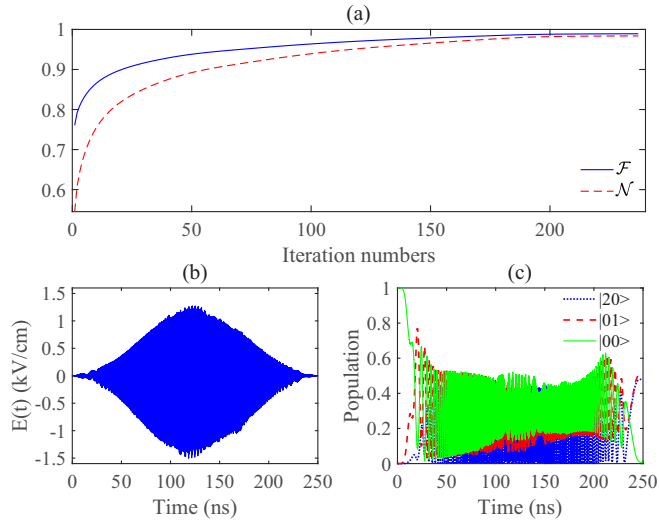
FIG. 3. (a) Fidelity and negativity of the systemic final state after applying the optimized control field for the transition of $\psi_i(t = 0) = |00\rangle \rightarrow \phi_f(T) = \frac{1}{\sqrt{2}}(|01\rangle + |20\rangle)$ as a function of the iteration number. (b) Converged laser pulse corresponding to the last iteration, for which the maximum amplitude is about 1.50 kV/cm. (c) Time-dependent populations of the wave function driven by the converged laser pulse for creating the target state $\phi_f(T) = \frac{1}{\sqrt{2}}(|01\rangle + |20\rangle)$.

FIG. 4. (a) Fidelity and negativity of the systemic final state after applying the optimized control field for the transition of $\psi_i(t = 0) = |00\rangle \rightarrow \phi_f(T) = \frac{1}{\sqrt{3}}(|01\rangle + |12\rangle + |20\rangle)$ as a function of the iteration number. (b) Converged laser pulse corresponding to the last iteration, for which the maximum amplitude is about 1.53 kV/cm. (c) Time-dependent populations of the wave function driven by the converged laser pulse for creating the target state $\phi_f(T) = \frac{1}{\sqrt{3}}(|01\rangle + |12\rangle + |20\rangle)$.

qutrit-qubit states, such as $\frac{1}{\sqrt{2}}(|10\rangle + |21\rangle)$, $\frac{1}{\sqrt{2}}(|11\rangle + |20\rangle)$, and $\frac{1}{\sqrt{2}}(|00\rangle + |21\rangle)$, can also be generated with high fidelity by optimal control and are not covered here again.

The qutrit-qutrit system is a straightforward extension of the qutrit-qubit system; thus, we turn to employ both SrO molecules as qutrits. In this way, the Hilbert space is extended to $3 \otimes 3$ from $3 \otimes 2$. Here, the target state is set to $\phi_f(T) = \frac{1}{\sqrt{3}}(|01\rangle + |12\rangle + |20\rangle)$, which is one of the maximally entangled states for the qutrit-qutrit system and is significant for superdense coding [56] and remote state preparation [57] in arbitrarily high dimensions. As shown in Fig. 4(a), both the fidelity and the negativity increase monotonously with the increasing number of optimizations and finally reach the convergence limit in an asymptotical way. Through 230 iterations, the values of both $\mathcal{F}$ and $\mathcal{N}/2$ are approximately equal to 0.992. The time profile of the optimal field at the 230th iteration is given in Fig. 4(b). The converged optimal control field can effectively steer the transformation of $|00\rangle \rightarrow \frac{1}{\sqrt{3}}(|01\rangle + |12\rangle + |20\rangle)$, as shown in Fig. 4(c). The final molecular populations after evolutions are about 0.005 for $|00\rangle$, 0.333 for $|01\rangle$, 0.312 for $|12\rangle$, and 0.349 for $|20\rangle$.

To further enlarge the Hilbert space consisting of pendular states, each SrO molecule with four pendular energy levels is used as a ququart. As before, an entangled state is required as the target state $\phi_f(T)$. Here, we suppose $\phi_f(T) = \frac{1}{2}(|00\rangle + |11\rangle + |22\rangle + |33\rangle)$. Figure 5(a) shows that the initial field takes 226 iterations to achieve the limit of convergence with $\mathcal{F} \approx 0.987$ and $\mathcal{N}/3 \approx 0.986$. Under the influence of the converged control field shown in Fig. 5(b), the populations of the final state after evolutions are about 0.261, 0.284, 0.218, and 0.228 for $|00\rangle$, $|11\rangle$, $|22\rangle$, and $|33\rangle$ [see Fig. 5(c)], respectively, nearly agreeing with those of the ideal target state.
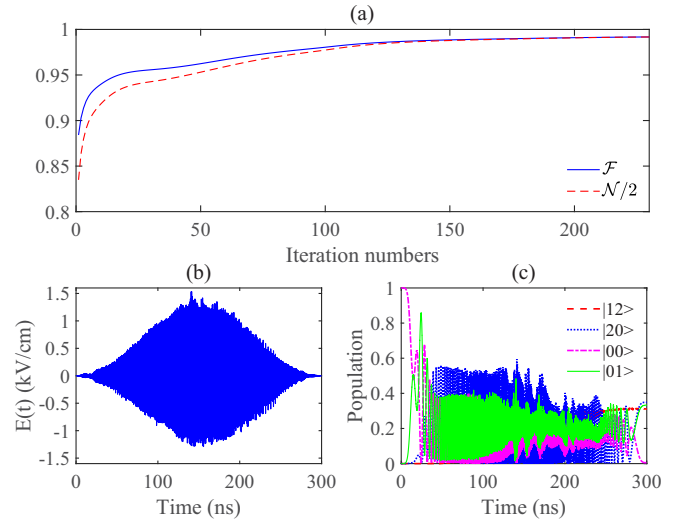
The above examples indicate that based on OCT, the pendular entangled states of qudit-qudit coupling can be realized with high fidelities, and the entanglement degree of the bimolecular systems can be enhanced effectively by designing suitable driving fields.
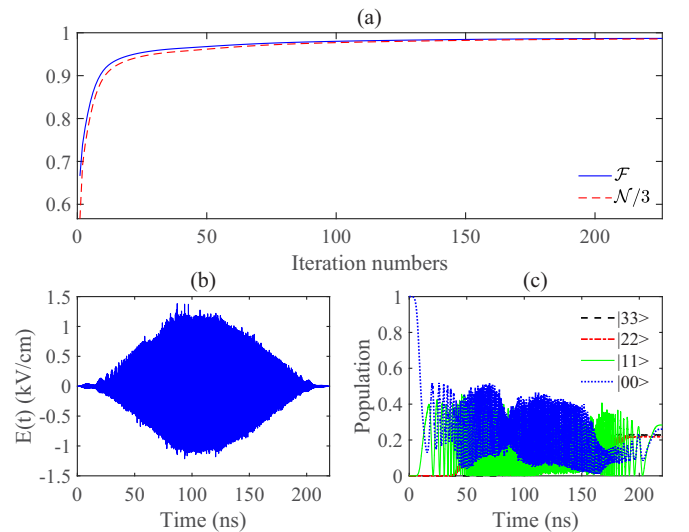

FIG. 5. (a) Fidelity and negativity of the systemic final state after applying the optimized control field for the transition of $\psi_i(t = 0) = |00\rangle \rightarrow \phi_f(T) = \frac{1}{2}(|00\rangle + |11\rangle + |22\rangle + |33\rangle)$ as a function of the iteration number. (b) Converged laser pulse corresponding to the last iteration, for which the maximum amplitude is about 1.38 kV/cm. (c) Time-dependent populations of the wave function driven by the converged laser pulse for creating the target state $\phi_f(T) = \frac{1}{2}(|00\rangle + |11\rangle + |22\rangle + |33\rangle)$.
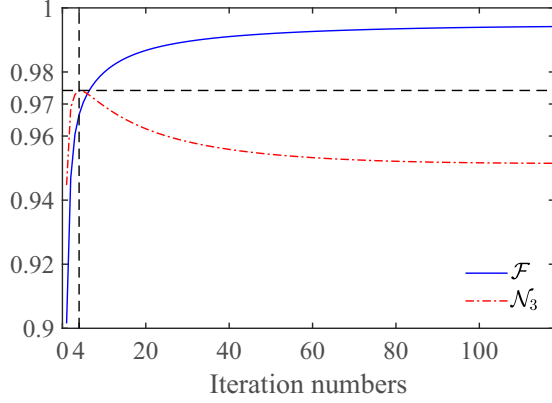
FIG. 6. Fidelity and tripartite negativity of the systemic final state after applying the optimized control field for the transition of $|000\rangle \rightarrow |W\rangle$ as a function of the iteration number. The maximum value of $\mathcal{N}_3$ is 0.974, which appears at the fourth iteration.

C. Three-qubit system

In general, the Hilbert space dimension can be increased not only by exploiting the multilevel system as qudits but also by increasing the number of qubits. Now, we consider a three-qubit system constructed of three coupled SrO molecules and design optimal optical fields to achieve three-qubit entanglement. For three polar molecules, there are two different arrangements: the linear type and the triangle type. For the linear type, the dipole-dipole interaction between next-nearest neighbors is relatively weak. Thus, we adopt the triangle-type configuration with an equal intermolecular distance of 75 nm. In this way, the dipolar interactions between any two SrO molecules are identical. For addressability, the external electric field intensities are set to 4.4, 5.5, and 6.6 kV/cm at the sites of three polar molecules. Moreover, to evaluate the performance of the control fields for generating triqubit entangled states, the negativity applied to the bipartite system needs to be generalized to the tripartite negativity [58]:

$$\mathcal{N}_3(\rho) = \sqrt[3]{\mathcal{N}_{i-jk}\mathcal{N}_{j-ik}\mathcal{N}_{k-ij}}. \quad (12)$$

Here, $\mathcal{N}_{A-BC} = \sum_i |\lambda_i(\rho^{T_A})| - 1$ [see Eq. (11)]. When $A = i, j, k$, BC corresponds to jk, ik, ij, respectively. In fact, the tripartite negativity is a geometric average of bipartite negativity. For a symmetric tripartite system, it can be simplified to the bipartite negativity of two arbitrary subsystems. It is known that the W and GHZ states are entangled states for two typical classes of three particles. The triqubit W state reads $|W\rangle = \frac{1}{\sqrt{3}}(|001\rangle + |010\rangle + |100\rangle)$, which is partially entangled with $\mathcal{N}_3(\rho) \approx 0.943$. The triqubit GHZ state reads $|GHZ\rangle = \frac{1}{\sqrt{2}}(|000\rangle + |111\rangle)$, which is maximally entangled with $\mathcal{N}_3(\rho) = 1$.

Now we take the W state and GHZ state as the target states for optimal control. Figure 6 shows the relations between the fidelity and the tripartite negativity as a function of the iteration number for the transition of $|000\rangle \rightarrow |W\rangle$. It can be seen that the fidelity of the final state increases gradually during the numerical optimization and reaches the maximum value of 0.994 after 118 iterations. However, the tripartite negativity displays a nonmonotonic behavior, and the maxi-
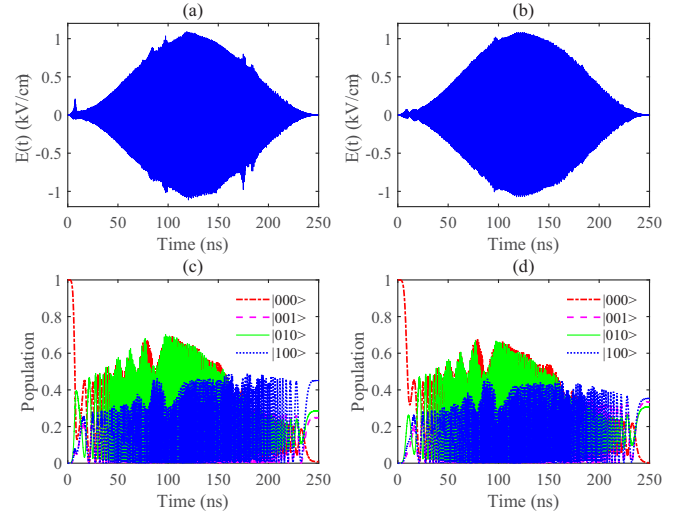

FIG. 7. (a) and (b) The optimized control fields corresponding to the fourth iteration and the last iteration for the transition of $|000\rangle \rightarrow |W\rangle$, for which the maximum amplitudes are about 1.11 and 1.08 kV/cm, respectively. (c) and (d) The time-dependent populations of the wave function driven by the optimized control fields at the fourth iteration and the last iteration, respectively.

mum value of 0.974 occurs at the fourth iteration. Thus, the fidelity and the entanglement do not always have to increase together as the optimization iterations increase. In general, when the target states are set to the maximally entangled states, both the negativity and the fidelity will gradually increase with the enhancement of optimization iterations. When the target states are partially entangled, the negativity and the fidelity may not follow the same behaviors. Figures 7(a) and 7(b) plot the control field versus the 4th iteration and the convergent field versus the 118th iteration, respectively, both of which are obtained by optimizing the initial field $E(t) = \sin^2(\pi t/T)\cos(\omega t)$, with $\omega = 2\pi \times 3.165 \times 10^{10}$ rad/s and $T = 250$ ns. The corresponding population evolutions are shown in Figs. 7(c) and 7(d), respectively. From the perspective of the final population distribution, the wave function driven by the convergent field is more approximate to the ideal W state.

Finally, the optimal control is performed for the transition of $|000\rangle \rightarrow |GHZ\rangle$. From Fig. 8(a), we can see that the fidelity and the tripartite negativity follow similar evolutionary trends, and the number of iterations necessary to reach convergence is 419. For the last iteration, $\mathcal{F} \approx 0.997$ and $\mathcal{N}_3 \approx 0.999$ can be achieved. The convergent control field with a frequency of 3.530×10^4 MHz and a duration of 200 ns is shown in Fig. 8(b). Moreover, Fig. 8(c) indicates that both of the final populations of $|000\rangle$ and $|111\rangle$ are very close to the desired value of 0.5, confirming the validity of the converged field. In addition, the populations for other basis states (e.g., $|010\rangle$) are almost restored to the initial value of zero after many oscillations, remaining unchanged after the converged laser pulse is applied.

It should be mentioned that in Ref. [32] the scheme for the entangling gate does not involve static electric fields but relies instead on magnetic and MW fields, and its fidelity is larger than 0.999. Moreover, the scheme takes into account
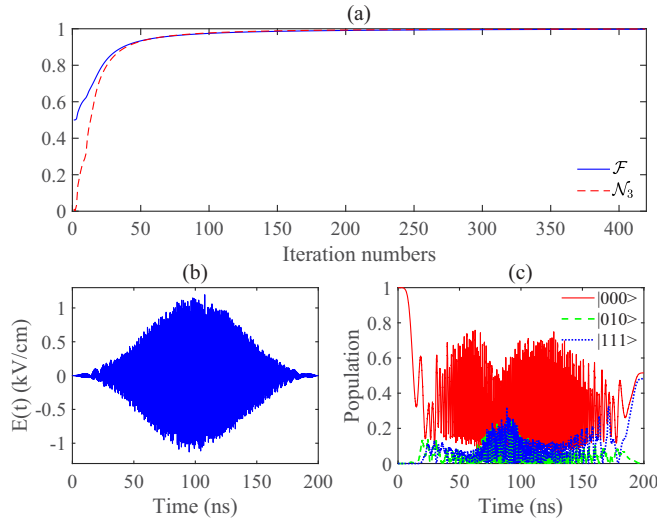
FIG. 8. (a) Fidelity and tripartite negativity of the systemic final state after applying the optimized control field for the transition of $|000\rangle \rightarrow |GHZ\rangle$ as a function of iteration number. (b) Converged laser pulse corresponding to the last iteration, for which the maximum amplitude is about 1.20 kV/cm. (c) Time-dependent populations of the wave function driven by the converged laser pulse for creating the target state $\phi_f(T) = |GHZ\rangle$.

the thermal excitation, the detuning, and the Rabi amplitude error, which is robust with respect to realistic experimental uncertainties. In principle, the two-qubit gate that the authors designed allows universal quantum computing, and their scheme can be generalized to realize triqubit W and GHZ states and other multiparticle entangled states.

IV. DISCUSSION AND SUMMARY

In this work, the SrO molecules have been used as candidate qudits due to the large dipole moments. It is worth emphasizing that for polar molecules with smaller dipole moments, our scheme can also behave well for generating entangled states, but longer control pulses and more iterations are required. Here, we choose CaF molecules as a carrier for testing, for which the dipole moment is about 3.1 debye. As shown in Fig. 9(a), when the pulse length is 250 ns, the fidelity of the entangled qutrit-qubit state of the coupled CaF molecules can reach only about 0.896 after 3305 optimization iterations, whereas the fidelity for SrO molecules can reach 0.989 after just 237 iterations. If the length of the pulse acting on the CaF molecules is increased to 500 ns, the fidelity can be enhanced to 0.979 after 1493 iterations. This means that the fidelity for the SrO molecules can more quickly tend to the limit of convergence with a shorter control pulse and its convergence value is larger.

It should be pointed out that the molecule spacing of 75 nm of molecules trapped in the nearest potential wells that we assumed in this study is difficult to realize and is significantly smaller than those achieved in current related experiments. As is well known, ∼500 nm is a typical spacing for molecules trapped in an optical lattice. However, the numerical calculation for spacing of 500 nm is beyond the capability of ordinary computers. This is because the optimization of the
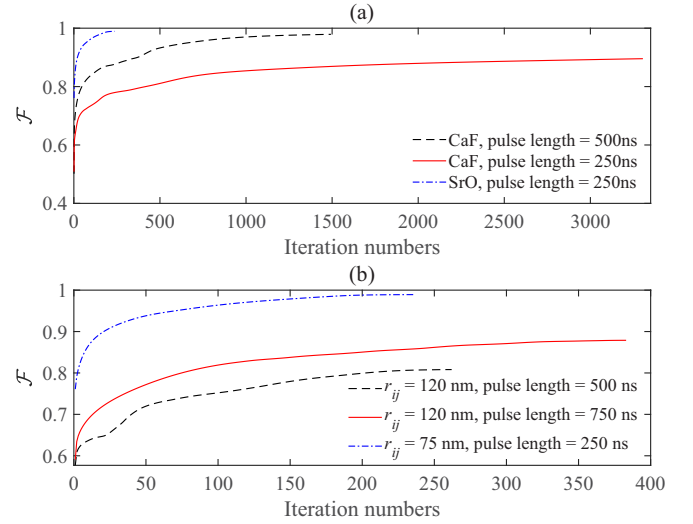

FIG. 9. (a) Fidelity of the final states driven by the optimized pulse with different pulse lengths as a function of iteration numbers for SrO and CaF molecules at the molecule spacing $r_{ij} = 75$ nm. (b) Fidelity of the final states driven by the optimized pulse with different lengths as a function of iteration numbers for the coupled SrO molecules at different molecule spacings r_{ij}. In both plots, the target state is set to the entangled qutrit-qubit state $\frac{1}{\sqrt{2}}(|01\rangle + |20\rangle)$.

control pulse needs multiple iterations and the time required for each iteration is proportional to the pulse length, whereas the necessary pulse length to guarantee high fidelity is inversely related to the dipole-dipole interaction. If the molecule spacing is set to 500 nm, the dipole-dipole interaction is very weak, which will require a long pulse duration and a long execution time in the numerical calculation. Here, we take the molecule spacing of $r_{ij} = 120$ nm as a test case. As shown in Fig. 9(b), under the optimized pulse with 500 ns the fidelity of the desired qutrit-qubit entangled state reaches only 0.808 after 262 iterations. When the pulse length is set to 750 ns, the fidelity can be enhanced to 0.879 after 383 iterations. It is found that the total computation time is much longer than that for the molecules with a spacing of 75 nm driven by an optimized pulse for 250 ns. However, the achieved fidelity is still far smaller than 1. To further enhance the fidelity, a longer pulse and computation time are required. Since the dipole-dipole interaction $V_{d-d}^{i,j} \propto 1/r_{ij}^3$, the increase in the necessary simulation time may be nonlinear as r_{ij} increases. Although the spacing of our testing is only 120 nm, it can be predicted that high-dimensional entangled states for polar molecules at $r_{ij} \sim 500$ nm can also be created under long enough control pulses obtained after the consumption of a lot of computing time.

To allow spectroscopic addressing of each dipole site, the external electric field needs to have sufficient intensity gradients at different molecule sites. As we know, the difference between transition frequencies of nearest-neighbor molecular bits is given by [59]

$$\Delta \nu = \frac{\Delta \varepsilon \mu}{\hbar} = \frac{g r_{ij} \mu}{\hbar}, \tag{13}$$

where $\Delta\varepsilon$ is the difference between the electric field intensities at the sites of two molecules, g is the gradient of ε, and $\hbar$ is the reduced Planck constant. Considering that $\Delta\nu = 100$ Hz is large enough to guarantee selective addressing of a particular qubit, if the spacing of the SrO molecules trapped in the optical lattices is $r_{ij} = 500$ nm, we obtain electric field gradient $g \approx 7.1 \times 10^{-2}$ V/cm^2.

We have studied how to apply OCT to generate various types of high-dimensional entangled states in the SrO molecular system under an electric field. To enlarge the dimension of Hilbert space, we have utilized multiple pendular states of SrO molecules as qudits and then enhanced the number of SrO molecules coupled via dipole-dipole interaction. Through numerical calculation, a series of optimal control fields was designed which can achieve the transfer from the systemic initial states to the desired target states. To improve the bipartite systemic entanglement, the target states were set to maximally entangled states of qutrit-qubit type, qutrit-qutrit type, and ququart-ququart type. It was found that the fidelity and negativity of the field-driven wave functions increase rapidly with the growth of the number of iterations. After enough iteration steps, convergent control fields for bimolecular systems can be obtained with high fidelities. Moreover, we have also successfully designed optimal control fields for the creation of the trimolecular W state and GHZ state. We found that the evolution trends of the fidelity and the tripartite negativity for the W state are not in good agreement with each other. To maximize the systemic entanglement, the iteration needs to be terminated in advance.

In this study, we have considered a molecule with four-level structure as the pendular ququart and each of three dipole-dipole coupled molecules as the pendular qubit. In principle, our scheme can be generalized to the case of more energy levels, more degrees of freedom, and more coupled ultracold molecules. Thus, our studies pave the way toward high-dimensional quantum information processing with polar molecules.

ACKNOWLEDGMENTS

[1] M. Erhard, M. Krenn, and A. Zeilinger, Advances in high-dimensional quantum entanglement, Nat. Rev. Phys. **2**, 365 (2020).

[2] D. Cozzolino, B. D. Lio, D. Bacco, and L. K. Oxenløwe, High-dimensional quantum communication: Benefits, progress, and future challenges, Adv. Quantum Technol. **2**, 1900038 (2019).

[3] Y. Wang, Z. Hu, B. C. Sanders, and S. Kais, Qudits and high-dimensional quantum computing, Front. Phys. **8**, 589504 (2020).

[4] H. Bechmann-Pasquinucci and W. Tittel, Quantum cryptography using larger alphabets, Phys. Rev. A **61**, 062308 (2000).

[5] N. J. Cerf, M. Bourennane, A. Karlsson, and N. Gisin, Security of Quantum Key Distribution Using d-Level Systems, Phys. Rev. Lett. **88**, 127902 (2002).

[6] E. T. Campbell, Enhanced Fault-Tolerant Quantum Computing in d-Level Systems, Phys. Rev. Lett. **113**, 230501 (2014).

[7] S. Ecker, F. Bouchard, L. Bulla, F. Brandt, O. Kohout, F. Steinlechner, R. Fickler, M. Malik, Y. Guryanova, R. Ursin, and M. Huber, Overcoming Noise in Entanglement Distribution, Phys. Rev. X **9**, 041042 (2019).

[8] D. DeMille, Quantum Computation with Trapped Polar Molecules, Phys. Rev. Lett. **88**, 067901 (2002).

[9] L. D. Carr, D. DeMille, R. V. Krems, and J. Ye, Cold and ultracold molecules: Science, technology and applications, New J. Phys. **11**, 055049 (2009).

[10] K. Mishima, K. Shioya, and K. Yamashita, Generation and control of entanglement and arbitrary superposition states in molecular vibrational and rotational modes by using sequential chirped pulses, Chem. Phys. Lett. **442**, 58 (2007).

[11] Q. Wei, S. Kais, B. Friedrich, and D. Herschbach, Entanglement of polar symmetric top molecules as candidate qubits, J. Chem. Phys. **135**, 154102 (2011).

[12] K.-K. Ni, T. Rosenband, and D. D. Grimes, Dipolar exchange quantum logic gate with polar molecules, Chem. Sci. **9**, 6830 (2018).

[13] V. V. Albert, J. P. Covey, and J. Preskill, Robust Encoding of a Qubit in a Molecule, Phys. Rev. X **10**, 031050 (2020).

[14] R. Sawant, J. A. Blackmore, P. D. Gregory, J. Mur-Petit, D. Jaksch, J. Aldegunde, J. M. Hutson, M. R. Tarbutt, and S. L. Cornish, Ultracold polar molecules as qudits, New J. Phys. **22**, 013027 (2020).

[15] Q. Wei, Y. Cao, S. Kais, B. Friedrich, and D. Herschbach, Quantum computation using arrays of N polar molecules in pendular states, ChemPhysChem **17**, 3714 (2016).

[16] M. Karra, K. Sharma, B. Friedrich, S. Kais, and D. Herschbach, Prospects for quantum computing with an array of ultracold polar paramagnetic molecules, J. Chem. Phys. **144**, 094301 (2016).

[17] Z.-Y. Zhang, J.-M. Liu, Z. Hu, and Y. Wang, Implementation of three-qubit quantum computation with pendular states of polar molecules by optimal control, J. Chem. Phys. **152**, 044303 (2020).

[18] S. Truppe, H. J. Williams, M. Hambach, L. Caldwell, N. J. Fitch, E. A. Hinds, B. E. Sauer, and M. R. Tarbutt, Molecules cooled below the Doppler limit, Nat. Phys. **13**, 1173 (2017).

[19] L. Anderegg, B. L. Augenbraun, E. Chae, B. Hemmerling, N. R. Hutzler, A. Ravi, A. Collopy, J. Ye, W. Ketterle, and J. M. Doyle, Radio Frequency Magneto-Optical Trapping of CaF with High Density, Phys. Rev. Lett. **119**, 103201 (2017).

[20] A. L. Collopy, S. Ding, Y. Wu, I. A. Finneran, L. Anderegg, B. L. Augenbraun, J. M. Doyle, and J. Ye, 3D Magneto-optical Trap of Yttrium Monoxide, Phys. Rev. Lett. **121**, 213201 (2018).

[21] S. Ding, Y. Wu, I. A. Finneran, J. J. Burau, and J. Ye, Sub-Doppler Cooling and Compressed Trapping of YO Molecules at μK Temperatures, Phys. Rev. X **10**, 021049 (2020).

[22] D. Mitra, N. B. Vilas, C. Hallas, L. Anderegg, B. L. Augenbraun, L. Baum, C. Miller, S. Raval, and J. M. Doyle, Direct laser cooling of a symmetric top molecule, Science **369**, 1366 (2020).

[23] S. F. Yelin, K. Kirby, and R. Côté, Schemes for robust quantum computation with polar molecules, Phys. Rev. A **74**, 050301(R) (2006).

[24] P. Yu, L. W. Cheuk, I. Kozyryev, and J. M. Doyle, A scalable quantum computing platform using symmetric-top molecules, New J. Phys. **21**, 093049 (2019).

[25] Q. Wei, S. Kais, B. Friedrich, and D. Herschbach, Entanglement of polar molecules in pendular states, J. Chem. Phys. **134**, 124107 (2011).

[26] M. Vatasescu, Entanglement between electronic and vibrational degrees of freedom in a laser-driven molecular system, Phys. Rev. A **88**, 063415 (2013).

[27] Z.-Y. Zhang and J.-M. Liu, Quantum correlations and coherence of polar symmetric top molecules in pendular states, Sci. Rep. **7**, 17822 (2017).

[28] T. Halverson, D. Iouchtchenko, and P.-N. Roy, Quantifying entanglement of rotor chains using basis truncation: Application to dipolar endofullerene peapods, J. Chem. Phys. **148**, 074112 (2018).

[29] I. Gonzalo and M. A. Antónb, Entangling non planar molecules via inversion doublet transition with negligible spontaneous emission, Phys. Chem. Chem. Phys. **21**, 10523 (2019).

[30] Z.-Y. Zhang, J.-M. Liu, Z. Hu, and Y. Wang, Optical control of entanglement and coherence for polar molecules in pendular states, Opt. Express **27**, 26588 (2019).

[31] E. Chae, Entanglement via rotational blockade of MgF molecules in a magic potential, Phys. Chem. Chem. Phys. **23**, 1215 (2021).

[32] M. Hughes, M. D. Frye, R. Sawant, G. Bhole, J. A. Jones, S. L. Cornish, M. R. Tarbutt, J. M. Hutson, D. Jaksch, and J. Mur-Petit, Robust entangling gate for polar molecules using magnetic and microwave fields, Phys. Rev. A **101**, 062308 (2020).

[33] X.-M. Hu, C. Zhang, B-H. Liu, Y. Cai, X.-J. Ye, Y. Guo, W.-B. Xing, C.-X. Huang, Y.-F. Huang, C.-F. Li, and G.-C. Guo, Experimental High-Dimensional Quantum Teleportation, Phys. Rev. Lett. **125**, 230501 (2020).

[34] Y.-H. Luo, H.-S. Zhong, M. Erhard, X.-L. Wang, L.-C. Peng, M. Krenn, X. Jiang, L. Li, N.-L. Liu, C.-Y. Lu, A. Zeilinger, and J.-W. Pan, Quantum Teleportation in High Dimensions, Phys. Rev. Lett. **123**, 070505 (2019).

[35] P. G. Kwiat, S. Barraza-Lopez, A. Stefanov, and N. Gisin, Experimental entanglement distillation and 'hidden' non-locality, Nature (London) **409**, 1014 (2001).

[36] A. C. Dada, J. Leach, G. S. Buller, M. J. Padgett, and E. Andersson, Experimental high-dimensional two-photon entanglement and violations of generalized Bell inequalities, Nat. Phys. **7**, 677 (2011).

[37] F. Arute, K. Arya, R. Babbush, D. Bacon, J. C. Bardin, R. Barends, R. Biswas, S. Boixo, F. G. S. L. Brandao, D. A. Buell, B. Burkett *et al.*, Quantum supremacy using a programmable superconducting processor, Nature (London) **574**, 505 (2019).

[38] C. Li, Y.-K. Wu, W. Chang, S. Zhang, Y.-F. Pu, N. Jiang, and L.-M. Duan, High-dimensional entanglement between a photon and a multiplexed atomic quantum memory, Phys. Rev. A **101**, 032312 (2020).

[39] X. Pan, S. Yu, Y. Zhou, K. Zhang, K. Zhang, S. Lv, S. Li, W. Wang, and J. Jing, Orbital-Angular-Momentum Multiplexed Continuous-Variable Entanglement from Four-Wave Mixing in Hot Atomic Vapor, Phys. Rev. Lett. **123**, 070506 (2019).

[40] D.-S. Ding, W. Zhang, S. Shi, Z.-Y. Zhou, Y. Li, B.-S. Shi, and G.-C. Guo, High-dimensional entanglement between distant atomic-ensemble memories, Light: Sci. Appl. **5**, e16157 (2016).

[41] J. Schneeloch, C. C. Tison, M. L. Fanto, P. M. Alsing, and G. A. Howland, Quantifying entanglement in a 68-billion-dimensional quantum state space, Nat. Commun. **10**, 2785 (2019).

[42] A. Tiranov, S. Designolle, E. Z. Cruzeiro, J. Lavoie, N. Brunner, M. Afzelius, M. Huber, and N. Gisin, Quantification of multi-dimensional entanglement stored in a crystal, Phys. Rev. A **96**, 040303(R) (2017).

[43] K. Kutluer, M. Mazzera, and H. de Riedmatten, Solid-State Source of Nonclassical Photon Pairs with Embedded Multimode Quantum Memory, Phys. Rev. Lett. **118**, 210502 (2017).

[44] W. Zhu, J. Botina, and H. Rabitz, Rapidly convergent iteration methods for quantum optimal control of population, J. Chem. Phys. **108**, 1953 (1998).

[45] H. Yu, T.-S. Ho, and H. Rabitz, Optimal control of orientation and entanglement for two dipole-dipole coupled quantum planar rotors, Phys. Chem. Chem. Phys. **20**, 13008 (2018).

[46] B. Friedrich and D. R. Herschbach, Spatial orientation of molecules in strong electric fields and evidence for pendular states, Nature (London) **353**, 412 (1991).

[47] P. Pellegrini, S. Vranckx, and M. Desouter-Lecomte, Implementing quantum algorithms in hyperfine levels of ultracold polar molecules by optimal control, Phys. Chem. Chem. Phys. **13**, 18864 (2011).

[48] J. Zhu, S. Kais, Q. Wei, D. Herschbach, and B. Friedrich, Implementation of quantum logic gates using polar molecules in pendular states, J. Chem. Phys. **138**, 024104 (2013).

[49] C. M. Rivera-Ruiz, E. F. de Lima, F. F. Fanchini, V. Lopez-Richard, and L. K. Castelano, Optimal control of hybrid qubits: Implementing the quantum permutation algorithm, Phys. Rev. A **97**, 032332 (2018).

[50] R. J. Spiteri, M. Schmidt, J. Ghosh, E. Zahedinejad, and B. C. Sanders, Quantum control for high-fidelity multi-qubit gates, New J. Phys. **20**, 113009 (2018).

[51] L. H. Coudert, Optimal orientation of an asymmetric top molecule with terahertz pulses, J. Chem. Phys. **146**, 024303 (2017).

[52] Q.-Q. Hong, L.-B. Fan, C.-C. Shu, and N. E. Henriksen, Generation of maximal three-state field-free molecular orientation with terahertz pulses, Phys. Rev. A **104**, 013108 (2021).

[53] Y. Kurosaki and K. Yokoyama, Quantum optimal control of the isotope-selective rovibrational excitation of diatomic molecules, Chem. Phys. **493**, 183 (2017).

[54] T. Baumgratz, M. Cramer, and M. B. Plenio, Quantifying Coherence, Phys. Rev. Lett. **113**, 140401 (2014).

[55] G. Vidal and R. F. Werner, Computable measure of entanglement, Phys. Rev. A **65**, 032314 (2002).

[56] X. S. Liu, G. L. Long, D. M. Tong, and F. Li, General scheme for superdense coding between multiparties, Phys. Rev. A **65**, 022304 (2002).

[57] J.-M. Liu and Y.-Z. Wang, Remote preparation of a two-particle entangled state, Phys. Lett. A **316**, 159 (2003).

[58] C. Sabín and G. García-Alcaine, A classification of entanglement in three-qubit systems, Eur. Phys. J. D **48**, 435 (2008).

[59] C. Lee and E. A. Ostrovskaya, Quantum computation with diatomic bits in optical lattices, Phys. Rev. A **72**, 062321 (2005).